Electronic Supplementary Information

A Hybrid Bulk-Heterojunction Photoanode for Direct Solar-to-Chemical Conversion

Liang Yao,†[a] Yongpeng Liu,†[a] Han-Hee Cho,[a] Meng Xia,[a] Arvindh Sekar,[a] Barbara Primera Darwich,[a] Rebekah A. Wells,[a] Jun-Ho Yum,[a] Dan Ren,[a] Michael Grätzel,[a] Néstor Guijarro[a] and Kevin Sivula*[a]

[a]Institute of Chemical Sciences and Engineering (ISIC), École Polytechnique Fédérale de Lausanne (EPFL), Station 6, 1015 Lausanne, Switzerland.

*Corresponding Author: kevin.sivula@epfl.ch

† These authors contributed equally to this work.

Contents

1. Supplementary Figures

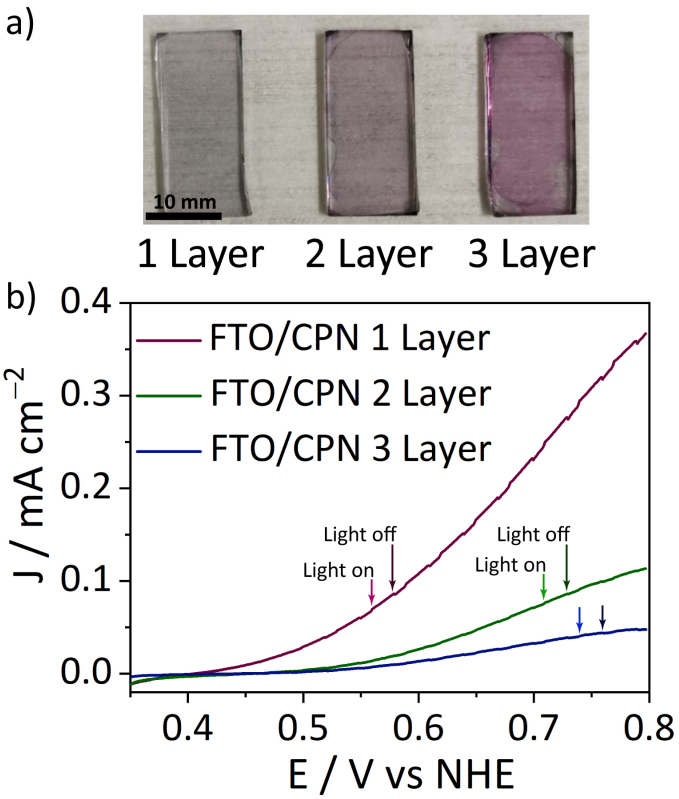

Figure S1. Planar FTO/CPN photoanodes. a) shows photographs of the planar FTO/CPN photoanodes with different thickness of CPN prepared by depositing multiple layers. Three layers of CPN leads to a thickness of 120 nm on top of the FTO (as shown below in **Figure S5**). b) shows linear sweep voltammetry (LSV) of the planar FTO/CPN photoanodes in 1 M iodide electrolyte (pH 1) under intermittent simulated solar illumination as indicated by selected light on/off cycles shown. The minor difference in the current density, J, between the light on and light off condition gives the photocurrent density J_{ph}.

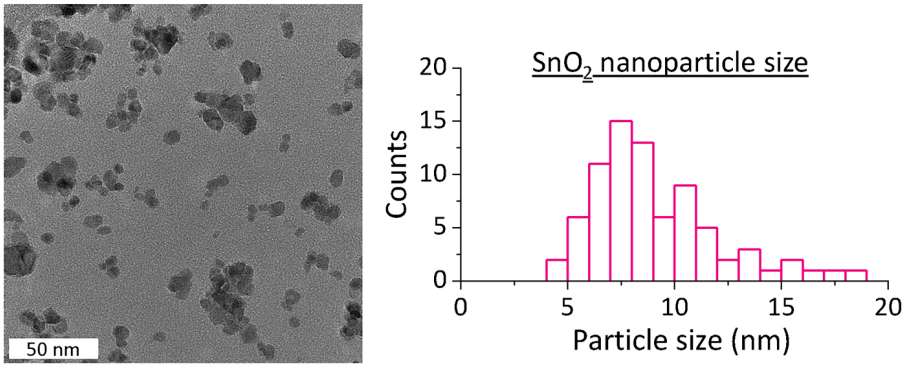

Figure S2. TEM image of SnO_2 nanoparticles and SnO_2 particle size distribution histogram extracted from the TEM image (accounting for overlapping).

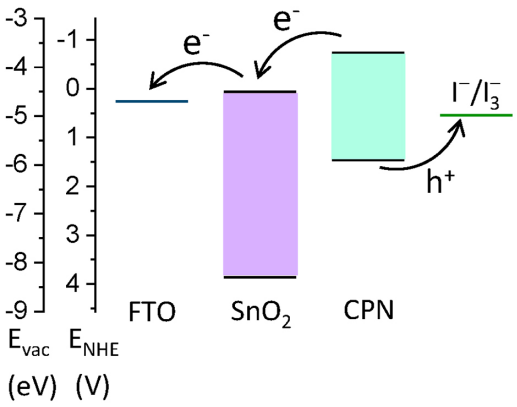

Figure S3. Energy level diagram against vacuum energy level and NHE at pH =0 of SnO_2 nanoparticles, CPN and I^-/I_3^- redox couple.

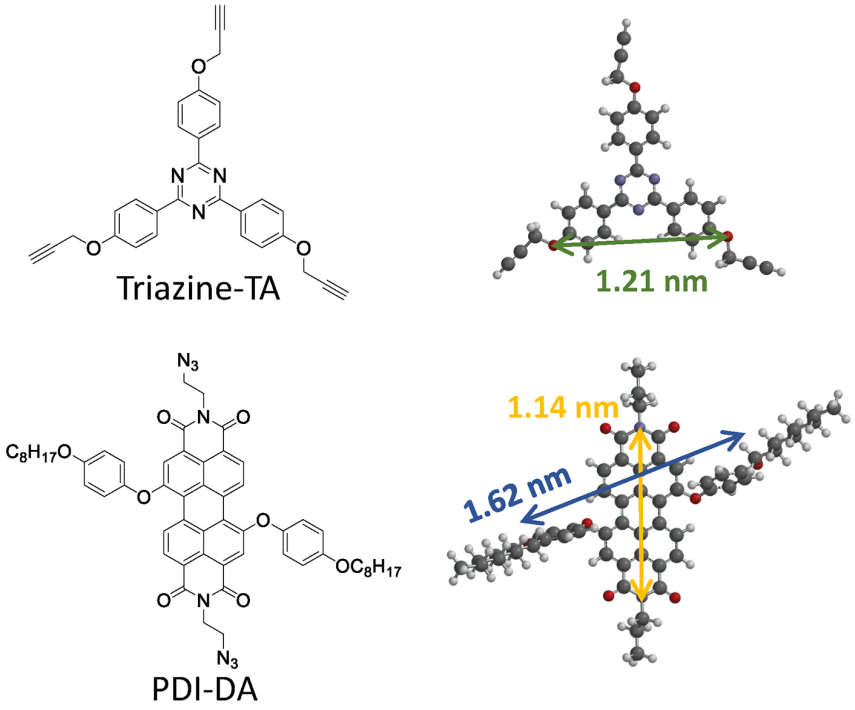

Figure S4. Molecular structure and optimized geometry of PDI-DA and Triazine-TA. The equilibrium geometry is simulated by Spartan 14' software package using the B3LYP/6-31G* basis set and the distance of conjugated part is displayed in the image.

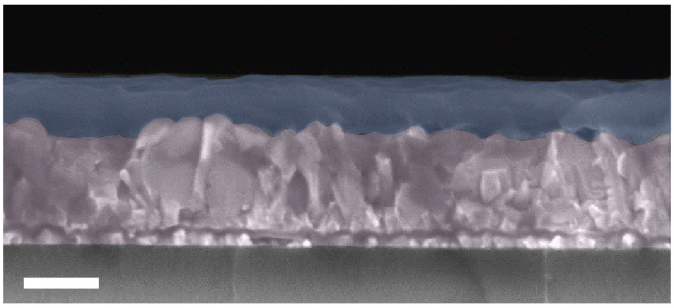

Figure S5. Cross sectional SEM image of CPN on FTO (3x monomer deposition/TAAC). The scale bar is 200 nm.

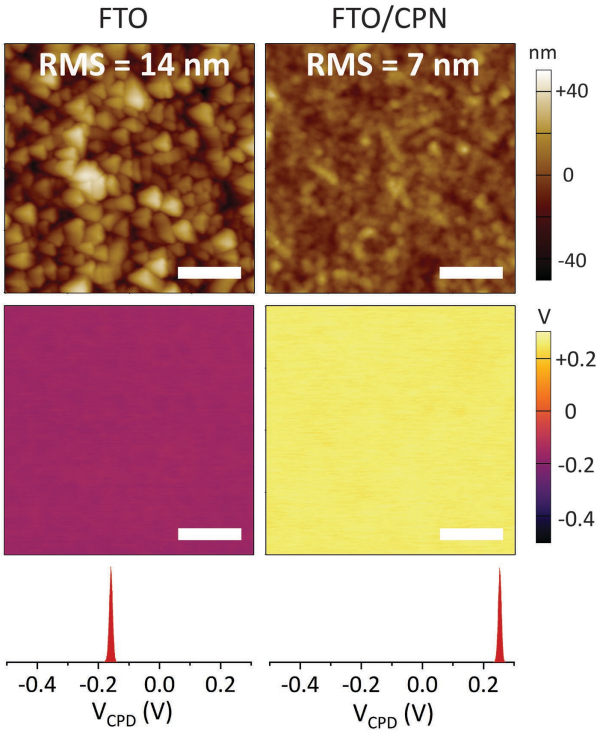

Figure S6. Morphological characterization of bare FTO and CPN on FTO (prepared with 1x monomer deposition/TAAC). Height topography, KPFM potential image, and contact potential difference (V_{CPD}) are shown in the top, middle and bottom panel, respectively. All the measurements were performed under dark ambient condition. The scale bar of the images is 500 nm.

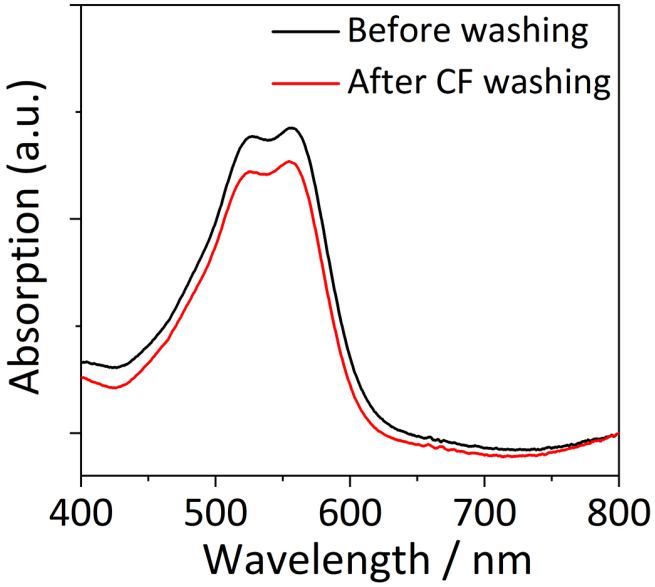

Figure S7. Comparison of the UV-vis absorption spectra of CPN:SnO_2 BHJ photoanode before and after chloroform (CF) washing (via a spin coating step). It can be seen that most of the absorption is kept after chloroform washing, indicating the TAAC reaction occurs after infiltrating PDI-DA and Triazine-TA into the SnO_2 nanoparticle film.

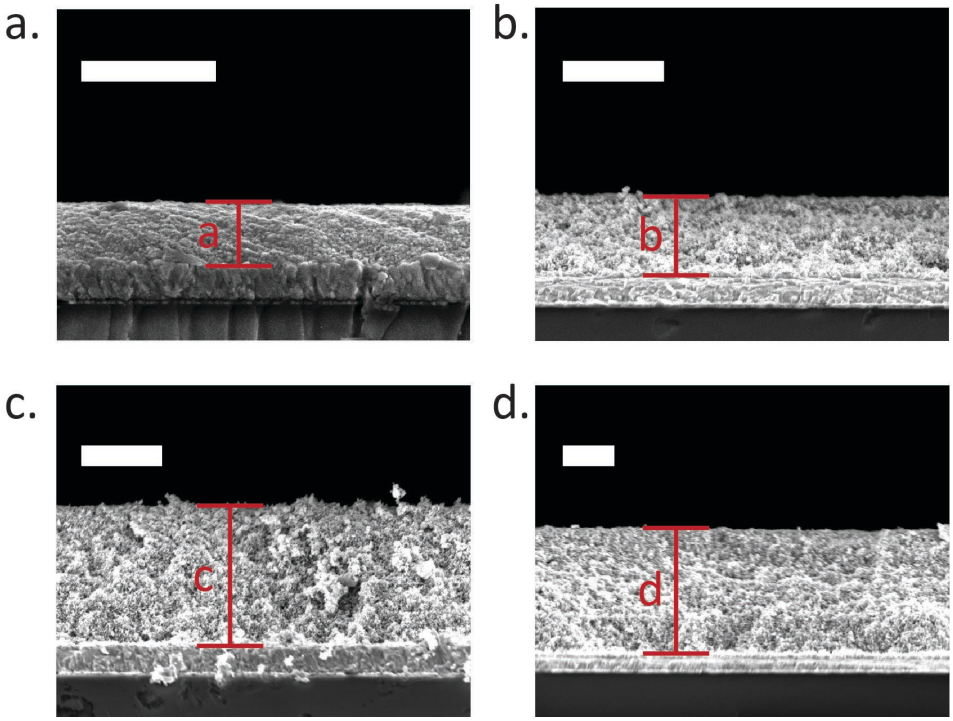

Figure S8. Cross-sectional SEM image of CPN:SnO_2 photoanodes. The scale bar in the images is 1 µm. The thickness is determined to be 480 nm (a), 770 nm (b), 1.77 µm (c), and 2.40 µm (d), respectively.

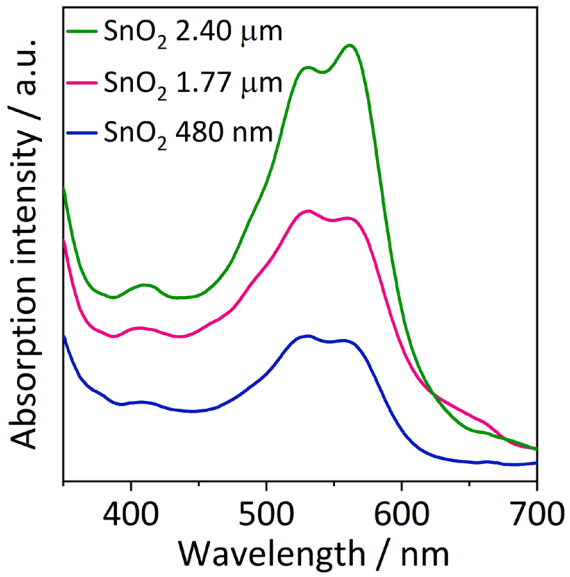

Figure S9. UV-vis absorption spectra of CPN:SnO_2 photoanode with SnO_2 nanoparticle thickness of 480 nm, 1.77 µm and 2.40 µm. PDI-DA and Triazine-TA were coated on top of SnO_2 nanoparticles with the same procedure. TAAC reaction was performed at 150 °C for 10 min to obtain CPN:SnO_2 BHJ.

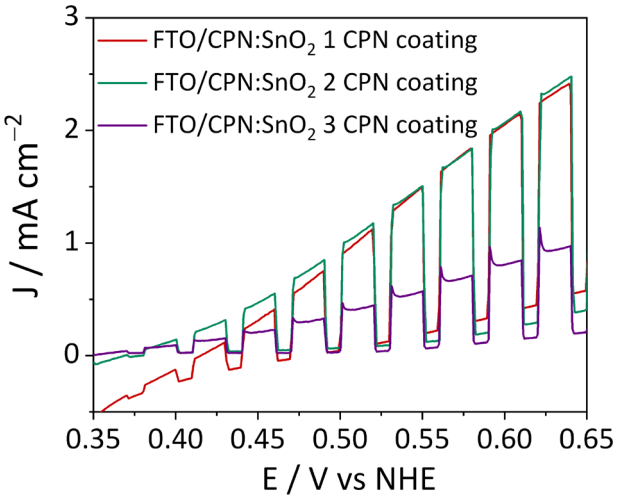

Figure S10. LSV scans of CPN:SnO_2 BHJ photoanodes in 1 M iodide electrolyte (pH 1) under intermittent 1 sun illumination. The m-SnO_2 layers have the same thickness in all cases (480 nm) and the number of monomer deposition/TAAC cycles was changed.

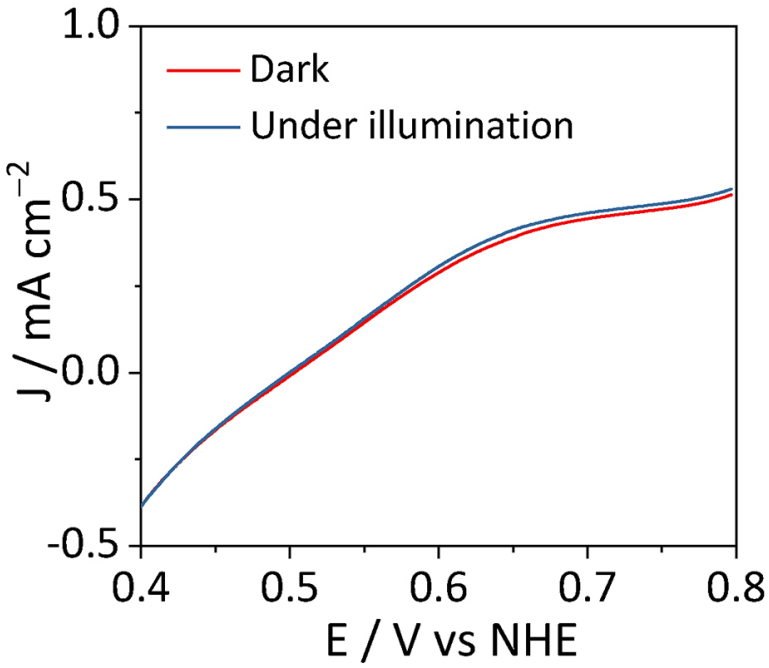

Figure S11. LSV scans of FTO/SnO_2 nanoparticle film (480 nm) under dark and 1 sun illumination. The electrolyte is 1 M iodide (I^-) at pH 1.

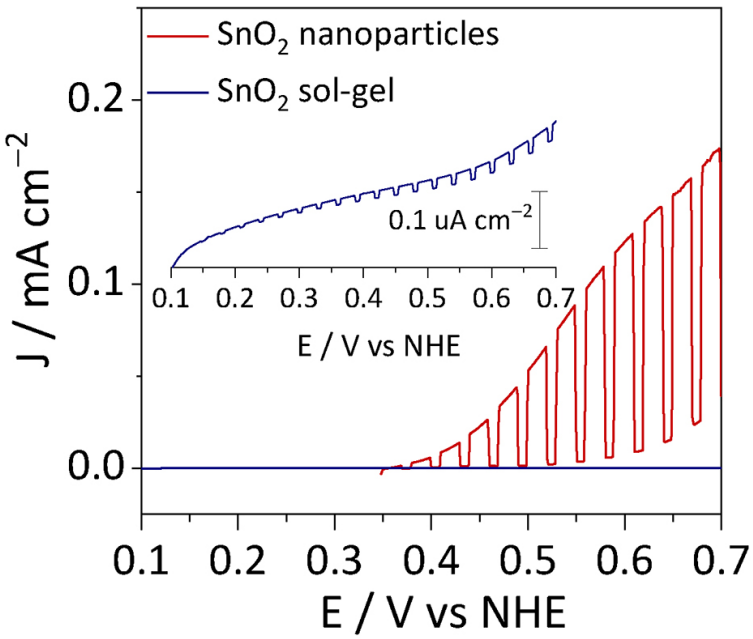

Figure S12. Comparison of LSV scans of CPN:SnO_2 BHJ (FTO/CPN:SnO_2) and SnO_2/CPN bilayer junction (FTO/SnO_2/CPN). 1x monomer deposition/TAAC was used for obtaining the CPN layer. The bilayer junction SnO_2 was prepared according to a previously-reported approach.[1] The SnO_2 thickness of both structures is 200 nm.

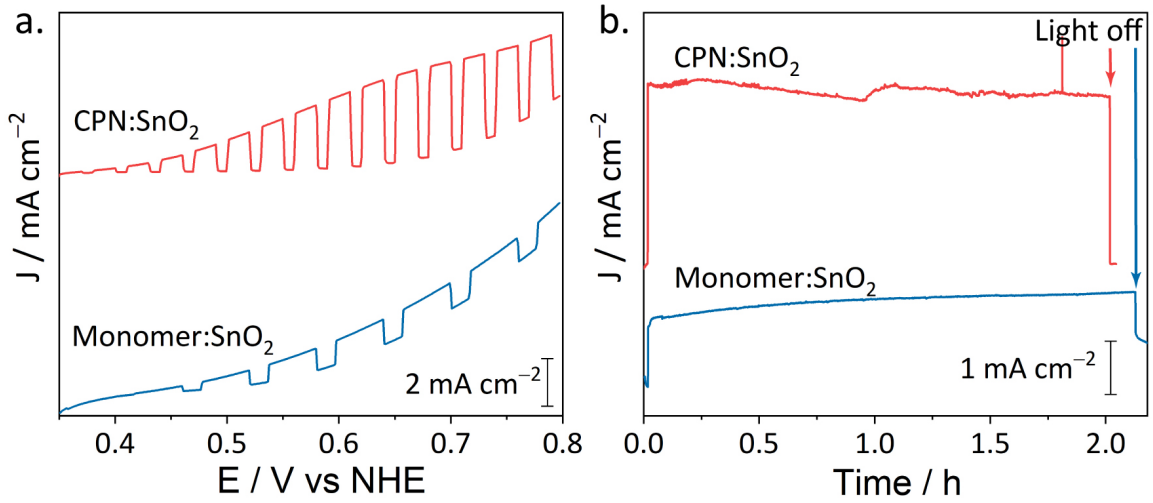

Figure S13. Performance of Triazine-TA and PDI-DA monomers:SnO_2 photoanode in 1 M iodide at pH 1. For the monomer:SnO_2 photoanode, the Triazine-TA:PDI-DA blend was coated onto SnO_2 nanoparticles (1.77 µm) with the same procedure but the heating to trigger TAAC reaction was not performed. a) LSV scans under intermittent illumination. b) CA test under continuous illumination at +0.75 V vs NHE. Illumination was switched on after 1 min stabilization in the dark.

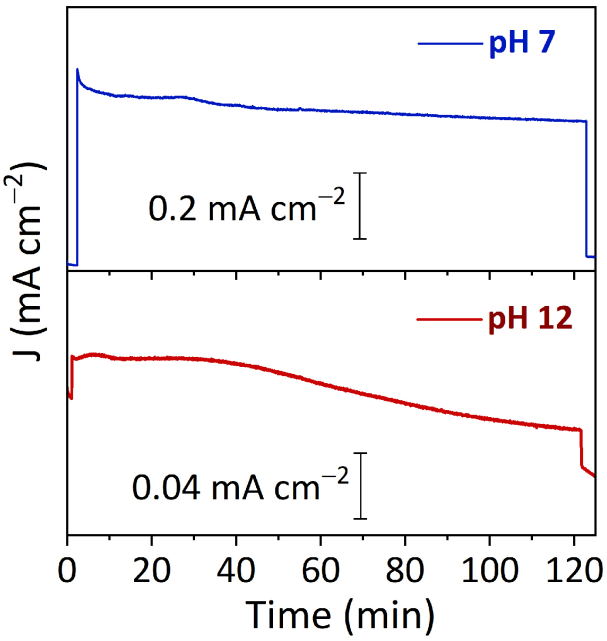

Figure S14. Chronoamperometry of the optimal CPN:SnO_2 photoanode in 1 M iodide at pH 7 and pH 12 under continuous illumination at +0.75 V vs NHE. Illumination was switched on after initial stabilization in the dark.

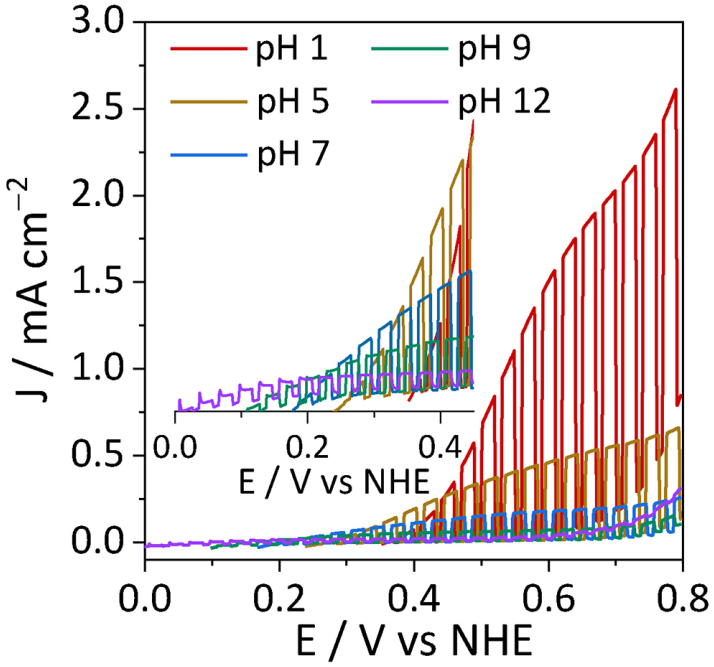

Figure S15. LSV scans of CPN:SnO_2 photoanode with 480 nm SnO_2 nanoparticle film in 1 M iodide at different pH.

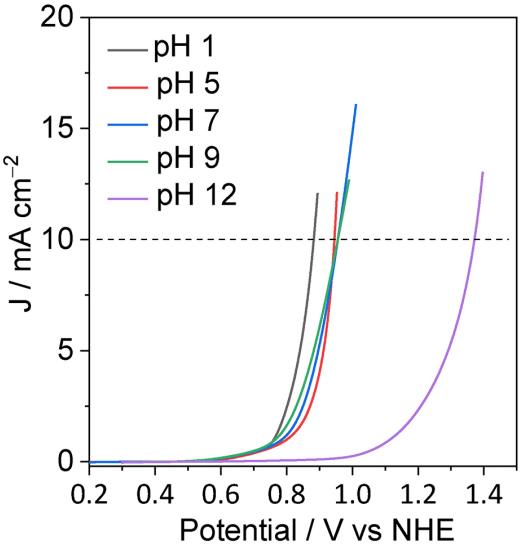

Figure S16. Polarization curves of bare FTO substrate after iR correction in 1 M iodide electrolyte at different pH (scan rate 1 mV s^{-1}).

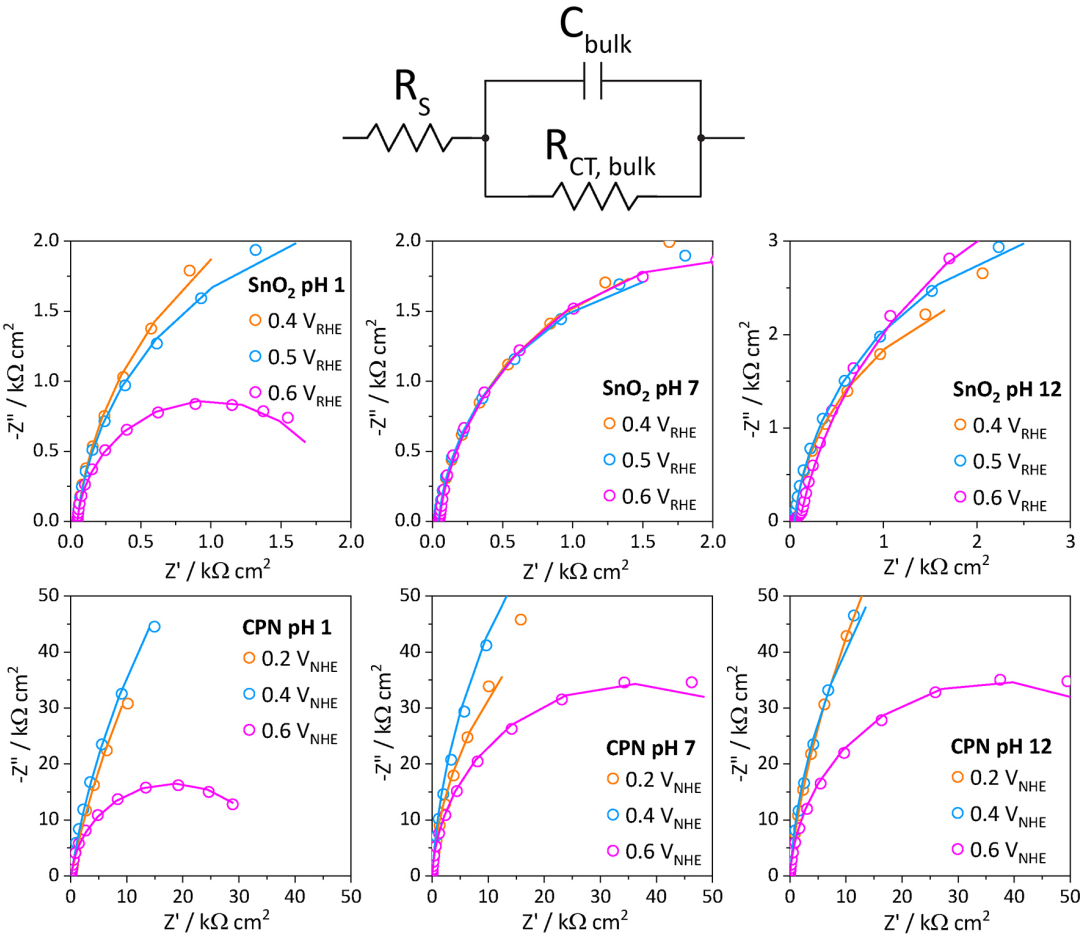

Figure S17. Nyquist plots of impedance measurements. The potential scale for SnO_2 and CPN is RHE and NHE, respectively. The equivalent circuit including series resistance R_S, charge transfer resistance from bulk $R_{CT, bulk}$, and bulk capacitance C_{bulk} was used to fit the impedance data. The fitted results were shown as the solid line in each graph.

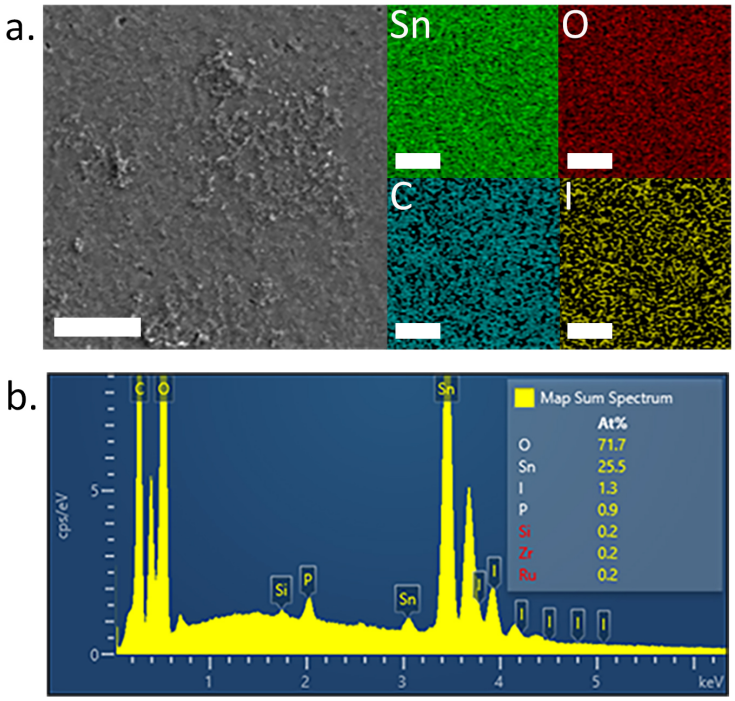

Figure S18. a) Top-down SEM image of CPN:SnO_2 photoanode after 5 h operation in 1 M HI at +0.54 V vs NHE. EDX mapping displays the element distribution (tin, oxygen, carbon and iodine). The scale bar is 10 µm. b) Elemental composition map sum spectrum of the SEM image. The relative percentage contributions by weight % are listed. The result indicates in-situ I_2 deposition occurs at the photoanode surface, due to the poor solubility of I_2 in water.

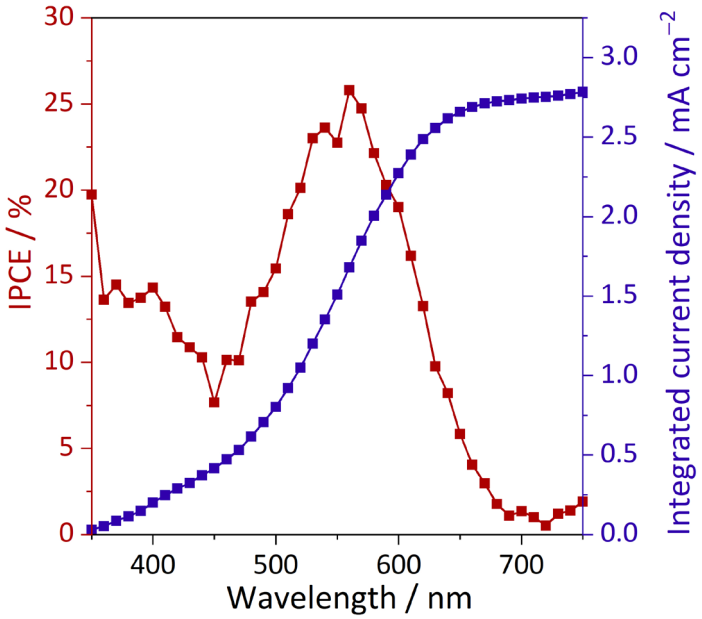

Figure S19. IPCE of CPN:SnO_2 photoanode at +0.54 V vs NHE in 1 M HI electrolyte. The integrated J_{ph} is shown with blue square markers.

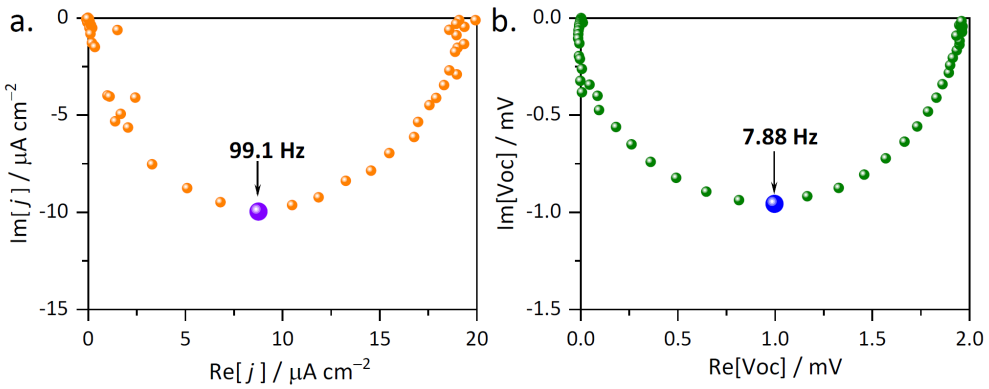

Figure S20. Nyquist plots of (a) IMPS and (b) IMVS response of the optimal CPN:SnO_2 BHJ photoanode. Both IMPS and IMVS were conducted in 1 M HI. IMPS was recorded at +0.54 V vs NHE and IMVS was recorded under open-circuit condition. IMPS/IMVS analysis reveals an electron diffusion coefficient (D_n) of 4.87×10^{-6} cm^2 s^{-1} and an electron diffusion length (L_n) of 3.14 μm, according to the model developed for DSSCs.

Details on charge carrier dynamics: To evaluate the charge carrier dynamics of our hybrid photoanode, we performed light modulation techniques, including intensity-modulated photocurrent spectroscopy (IMPS) and intensity-modulated photovoltage spectroscopy (IMVS) on the optimal CPN:SnO_2 BHJ photoanode with m-SnO_2 thickness of 1.77 μm, using 1 M HI as electrolyte. IMPS and IMVS are spectroelectrochemical techniques to investigate carrier transport/recombination, and have been widely applied in photovoltaic devices, such as dye-sensitized solar cells (DSSCs), perovskite solar cells and organic solar cells. Recently, IMPS/IMVS have been considered as emerging techniques for revealing carrier dynamics of solar water splitting devices. The Nyquist plots of IMPS and IMVS response are shown in Figure S20. It can be observed that Nyquist plots of IMPS and IMVS of CPN:SnO_2 photoanode could follow the model that developed in DSSCs.[2] We suppose this is rational, as HI oxidation is a kinetic favorable two-electron transfer reaction, which is analogous with the case in DSSCs and different from the four-electron transfer OER. As highlighted in Figure S20a, the characteristic frequency ($f_{min,IMPS}$) at the minimal point of IMPS response is correlated to the mean transit time for photogenerated electrons:

$$\tau_d = \left(2\pi f_{min,IMPS}\right)^{-1} = 1.61 \text{ ms}$$

Likewise, in Figure S20b the first-order electron lifetime (τ_n) can be estimated from the characteristic frequency ($f_{min,IMVS}$) in IMVS response:

$$\tau_n = \left(2\pi f_{min,IMVS}\right)^{-1} = 20.21 \text{ ms}$$

Combining the time constant obtained from IMPS and IMVS analysis, electron diffusion coefficient (D_n) and electron diffusion length (L_n) of CPN:SnO_2 photoanode can be estimated by:

$$D_n = \frac{d^2}{4\tau_d}$$

$$L_n = \sqrt{D_n \tau_n}$$

where d is the film thickness (1.77 μm). D_n and L_n are found to be around 4.87×10^{-6} cm^2 s^{-1} and 3.14 μm, respectively. The value of L_n is larger than d, ensuring the electron diffusion across the film.

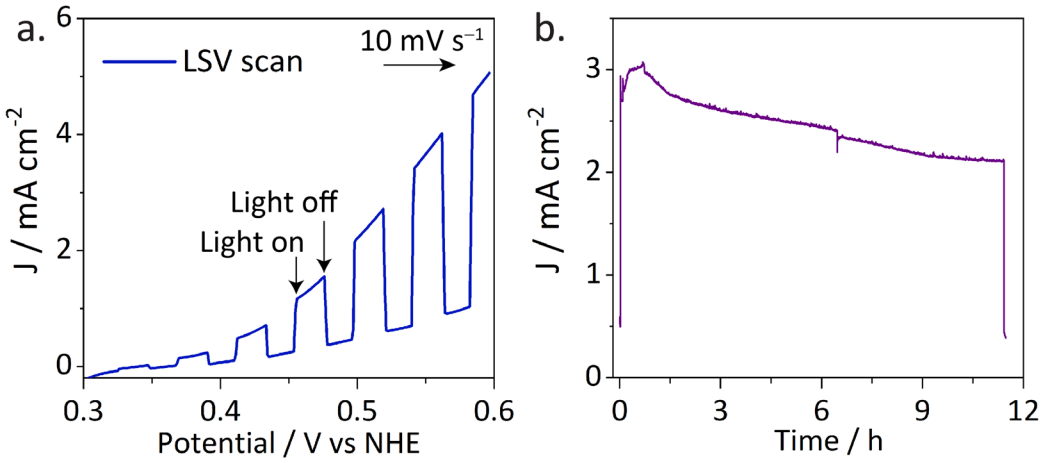

Figure S21. PEC test of another individual CPN:SnO_2 photoanode in 1 M HI for the quantification of I_3^- and H_2. a) LSV scan and b) 11 .4 h CA test at +0.54 V vs NHE under 1 sun illumination.

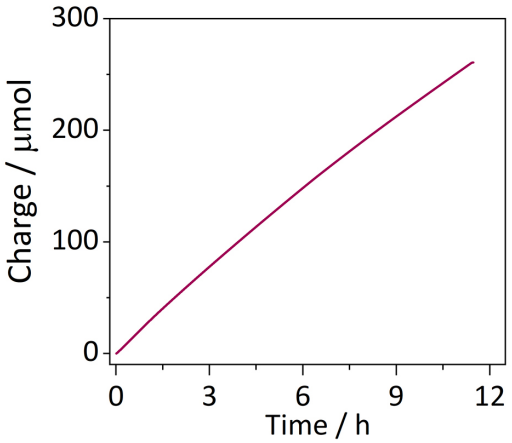

Figure S22. The number of electrons (µmol) calculated from 11.4 h CA test as a function of time. The total electron amount is 260.6 µmol.

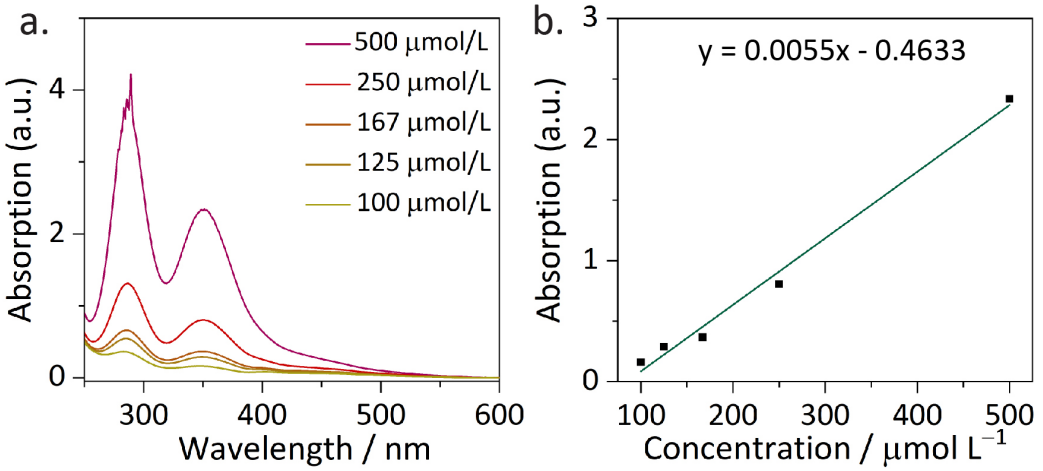

Figure S23. I_3^- amount quantification. a) UV absorption spectra of standard I_3^- solution with specific concentrations. b) Absorption intensity at 350 nm as a function of I_3^- concentration. A linear regression was used to fit the results (R^2 = 0.99). The absorption intensity at 350 nm of the electrolyte with 1/50 dilution (shown in Figure 5c in the main text) is 1.664, corresponding to a concentration of 386.8 µmol L^{-1}.

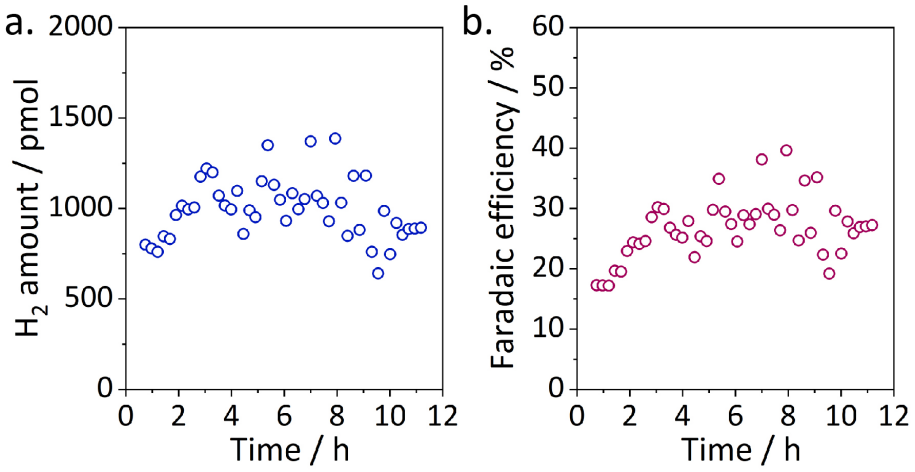

Figure S24. Hydrogen amount (a) and hydrogen evolution Faradaic efficiency (b) as a function of operation time.

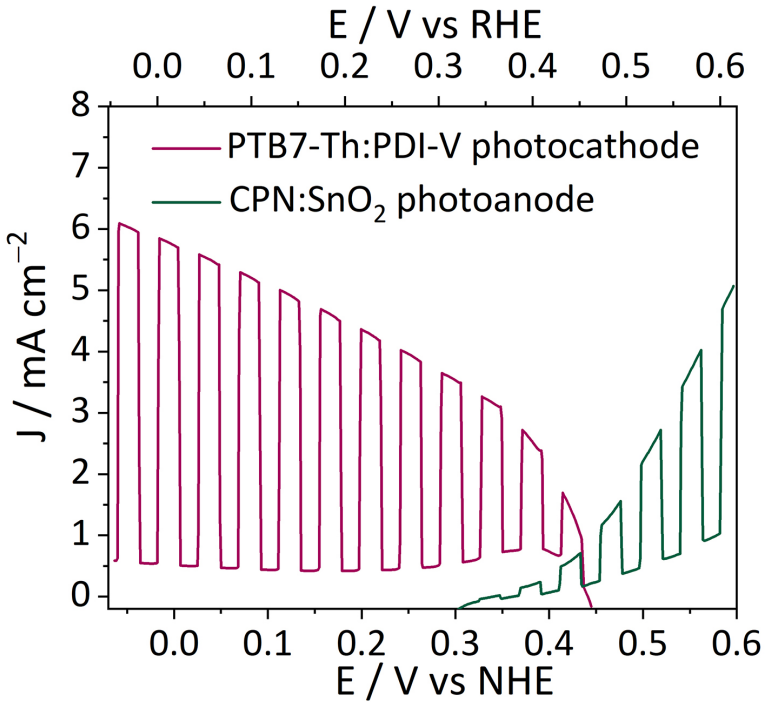

Figure S25. LSV scan of PTB7-Th:PDI-V photocathode and CPN:SnO_2 photoanode in 1 M HI under intermittent 1 sun illumination.

2. Supplementary Table

Table S1. Reported organic semiconductor photoanodes for solar-to-chemical conversion

Publication	Starting material	Product	Photoanode structure	Initial J_{ph}	Demonstrated operation time
This work	**I^-**	**I_3^-**	**FTO/CPN:SnO_2**	**3.3 mA cm^{-2} @0.54 V vs NHE**	**29 h @0.54 V vs NHE**
Chem. Mater., **2018**, 30, 324	H_2O	O_2	FTO/ZnO/$PC_{71}BM$/ZnO	≈60 μA cm^{-2} @1.23 V vs RHE	~940 s[a] @1.23 V vs RHE
Mater. Chem. Front., **2018**, 2, 2021	H_2O	O_2	FTO/TiO_2/C12	≈30 μA cm^{-2} @1.2 V vs RHE	90 s[a] @1.2 V vs RHE
ChemistrySelect, **2017**, 2, 4522	H_2O	O_2	ITO/PTEB	≈5 μA cm^{-2} @1.5 V vs RHE	Not reported
J. Am. Chem. Soc., **2015**, 137, 15338	H_2O	O_2	FTO/BBL/Ni–Co	≈30 μA cm^{-2} @1.23 V vs RHE	30 min[a] @1.23 V vs RHE
ACS Appl. Mater. Interfaces, **2014**, 6, 13367	H_2O	O_2	ITO/PMPDI/CoO_x	≈150 μA cm^{-2} @1.56 V vs RHE	300 s[a]
Angew. Chem. Int. Ed., **2012**, 124, 1943	H_2O	O_2	ITO/PTTh-2:MnPor	≈20 μA cm^{-2} @1.51 V vs RHE	700 s[a] @1.51 V vs RHE
Sci. China Chem., **2012**, 55, 1953	H_2O	O_2	ITO/PTCDA/PTCDA:$PC_{61}BM$/$PC_{61}BM$	≈160 μA cm^{-2} @1.16 V vs RHE	~1000 s[a] @1.16 V vs RHE
Angew. Chem. Int. Ed., **2006**, 45, 2778	H_2O	O_2	ITO/PTCBI/CoPc	≈20 μA cm^{-2} @1.2 V vs RHE	Not reported
J. Electroanal. Chem., **2006**, 587, 127	H_2O	O_2	ITO/PTCBI/H_2Pc/Nf-IrO_2	≈6 μA cm^{-2} @1.19 V vs RHE	1.5 h[b] @1.19 V vs RHE
RSC Adv., **2015**, 5, 46325	N_2H_4	N_2	ITO/PTCBI/CoPc/Nf	≈135 μA cm^{-2} @1.15 V vs RHE	1 h[b] @1.15 V vs RHE
Chem. Commun., **2014**, 50, 1950	N_2H_4	N_2	ITO/C_{60}/ZnPc/Nf	≈178 μA cm^{-2} @1.15 V vs RHE	1 h[b] @1.15 V vs RHE
Chem. Commun., **2019**, 55, 12491	RS^-	$RS^{\bullet-}$	ITO/ZnO/P3HT:PCBM/ZnPc	32 μA cm^{-2} @0.85 V vs RHE	Not reported
Phys. Chem. Chem. Phys., **2008**, 10, 1562	RS^-	$RS^{\bullet-}$	ITO/PTCBI/H_2Pc	≈300 μA cm^{-2} @0.79 V vs RHE	12 min[a] @0.79 V vs RHE
J. Electroanal. Chem., **2007**, 599, 65	RS^-	$RS^{\bullet-}$	ITO/C_{60}/H_2Pc	≈530 μA cm^{-2} @1.09 V vs RHE	4 min[a] @1.09 V vs RHE

[a] The operation time is extracted from the I–t curve under illumination at the specific potential.
[b] Overall product amount was checked after operation but I–t curve under illumination was not provided in the paper.

3. Supplementary References

1. W. Ke, G. Fang, Q. Liu, L. Xiong, P. Qin, H. Tao, J. Wang, H. Lei, B. Li, J. Wan, G. Yang and Y. Yan, *J. Am. Chem. Soc.*, 2015, **137**, 6730.
2. J. Krüger, R. Plass, M. Grätzel, P. J. Cameron and L. M. Peter, *J. Phys. Chem. B*, **2003**, 107, 7536–7539.